Renewable Energy 198 (2022) 283–295

Contents lists available at ScienceDirect

Renewable Energy

journal homepage: www.elsevier.com/locate/renene

Developing a new wind dataset by blending satellite data and WRF model wind predictions

Nadia Salvação [a], Abderrahim Bentamy [b], C. Guedes Soares [a,*]

[a] Centre for Marine Technology and Ocean Engineering (CENTEC), Instituto Superior Técnico, Universidade de Lisboa, Av. Rovisco Pais, 1049-001, Lisboa, Portugal
[b] Laboratoire Spatial et Interfaces Air-Mer (IFREMER), Centre Bretagne - ZI de la Pointe du Diable, CS 10070-29280, Plouzané, France

ARTICLE INFO

Keywords:
WRF
Satellite wind
Blended data
Wind energy

ABSTRACT

This paper presents an approach to improve wind datasets developed using the regional atmospheric model Weather Research Forecasting by combining its predictions with remotely sensed wind observations in enhanced wind speed analyses that leads to blended winds. In this study, satellite data derived from scatterometers, radiometers, and synthetic aperture radar are used. The spatial and temporal features of each wind product are thoroughly analysed. For the probabilistic evaluation of their skill, comprehensive comparisons with available buoy data are carried out. The statistical analysis shows that the combined use of satellite and numerical weather prediction model data improves the agreement with buoy measurements, demonstrating the added value of using the blended product. As an application of the method, new improved satellite wind speeds are presented in the form of a wind energy assessment along the Iberian coastal area. From inspection of the provided wind power maps, northern and central regions emerge as the most promising areas for wind harnessing offshore despite some seasonal variations. Finally, potential wind farm sites are provided, along with insights into multi-year wind speed distribution. The results show how the new dataset can be used for the selection of promising areas for wind exploitation.

1. Introduction

Improving the skill of wind speed predictions and understanding its regional patterns, brings numerous economic and technical advantages [1,2], in particular for the wind energy industry, which is expanding offshore at a fast pace [3–6]. In the present day, the spatial distribution of wind resources is still a major element for the siting of offshore wind parks [7–10]. Having adequate climate services and adopting the existing ones persists as a big challenge for the wind energy sector [11].

Several wind datasets are publicly available, allowing for a quick evaluation of the regions with greater wind exploitation potential. Examples are reanalysis datasets such as Era-interim [12] and Era 5 [13] or MERRA-2 [14]. However, these lack the necessary spatial resolution and are not capable of addressing each site's unique local climatic characteristics which highly affects wind power peaks and ramps predictions [15]. The Global Wind Atlas and the New European Wind Atlas are also widely used tools for wind energy assessment and have even been used in combination with reanalysis data for bias correction, but research found some versions of this product to be inefficient in improving simulation quality [16].

Similarly, numerical weather prediction (NWP) models are also one of the most widely used tools for wind assessment [17,18]. Various studies have further pointed out the WRF model as an effective wind assessment tool [19,20]. WRF has been proved to be a useful model to assess wind resources in various countries such as Oman [21], Northern Europe [22], Iceland [23], Portugal [24], and therefore it has been chosen to perform this study.

Although several resource assessment systems have been developed to provide accurate estimates of the available wind power across different regions, the current deterministic NWP models regardless of their demonstrated skill, have several limitations as they only represent a single wind trajectory for each site and consequently one future scenario of the energetic conditions and high dependence upon the initial conditions. Ensembles of simulations have been proved to improve this situation [25–27].

Despite its indisputable capabilities, NWP models still have a large margin for improvement. Novel improved methods can significantly reduce the risk and uncertainty for both the planning and maintenance stages of wind parks. A new design for wind and wind power forecasting designed by combining the results of WRF with fuzzy clustering,

* Corresponding author.
E-mail address: c.guedes.soares@centec.tecnico.ulisboa.pt (C. Guedes Soares).

https://doi.org/10.1016/j.renene.2022.07.049
Received 12 May 2021; Received in revised form 7 July 2022; Accepted 9 July 2022
Available online 20 July 2022

association rule and optimization methodologies can be effective in reducing the uncertainty of wind farm forecasting [28]. In this study, the strengths that NWPs offer are combined with satellite data to improve their skill.

Therefore, combining NWP models with other sources of information can diminish the uncertainty of wind speed forecasts, especially if they have been tuned to give the most accurate conditions for a specific site. To take advantage of the strengths of multiple products, the joint use of distinct wind data sources tailored to the needs of each application has been widely employed over the last years [29–31]. A study [32] reconstructed one year of wind data from multiple satellite information and the WRF model to analyse the offshore wind resources over the South China Sea. The developed methodology provides a valuable tool for a well-informed site selection. This is of major interest for offshore areas where few in situ observations are available. Despite the demonstrated capabilities of NWP models, there are numerous advantages of using other sources of information. For instance, remote sensing data is capable of resolving fine-scale structures not fully captured by these models [33].

Satellite information has been recently used to assess the spatial variability of global ocean wind resources [34,35]. While satellite data contribute to spatial and temporal coverage, buoy data consists of a long and accurate time series of wind observations capable of describing the true wind conditions and providing information on the diurnal and seasonal/annual variability of the wind resource.

As concerns the Portuguese coastal zone, the study area considered in this work, the need for improved understanding of the wind patterns along the Iberian coastal zone drove several works that aimed at determining the most suitable areas for wind exploitation. Satellite data confirm that the Portuguese coastline has the potential to generate large amounts of electricity [36,37] showing that four main areas with homogeneous wind conditions can be devised on the Portuguese coast [35]. For example, a 10-year hindcast for the Iberian Peninsula coast demonstrated the WRF model's ability to express the local wind across the selected domain [24]. Also, for the Iberian Peninsula, another study [38] presents projections of future climate scenarios using a set of models that proved to successfully hindcast inland and offshore winds. The statistical properties of the data were analysed and it was shown that four main areas with homogeneous wind conditions could be devised on the Portuguese coast [39]. To address the challenges of the most commonly used wind resource assessment methods, this study aims to provide an accurate wind product capable of improving the existing data and provide accurate local resource estimation using two of the most accurate sources of wind data, numerical models and satellite data.

For this purpose, in this work, surface wind observations, retrieved from several satellite scatterometer and radiometer measurements, are combined with a 9-year (2004–2012) wind hindcast produced by the WRF model, resulting in new time series of blended wind estimates. The main strength of this method is that it uses the most suitable model configuration for the area of interest in combination with accurate satellite data that can correct the known deficiencies of NWP models such as wind magnitude bias. After validating the blended winds against a dataset of wind measurements obtained from a network of meteorological buoys, the temporal and spatial variability along the Iberian coast is examined in more detail.

The annual and seasonal variability as well as the mean extreme wind speed thresholds are also presented. The statistical characterization of wind power errors is performed. In this framework, the extreme wind speed in a given return period is used as a reference for survivability studies of the floating wind devices. The statistical percentile technique (90%, 95%, and 99%) and maxima over a specific period are some of the most commonly employed approaches to determine such a reference value [40]. To that end, the spatial distribution of the 99th percentile of the yearly wind speed is also mapped. The final aim is to build a new dataset of winds to produce high-resolution wind maps that can be used as a site selection tool for offshore and coastal projects.

This paper is organized in the following manner: section 2 briefly discusses the WRF model, the satellite analyses, buoy data and its agreement with observations; section 3 provides information about the Iberian coast wind patterns, the seasonal and intra-annual variations and extreme distribution of the wind. A comprehensive analysis of renewable energy follows in section 4 along with energy maps able to describe the available resources. Finally, a brief discussion of the results is presented in section 5.

2. Data

2.1. In-situ wind measurements

The main source of surface wind used is from buoys located in the Atlantic Ocean along the North of Spain (South of Biscay Bay), western areas of Spain and Portugal, and Southwest of Spain (Table 1). Buoy data are provided by Puertos Del Estado (Spain), Xunta De Galicia (Spain), and Instituto Hidrográfico (Portugal). They are made available as Copernicus Marine Environment Monitoring Service CMEMS (marine.copernicus.eu) products. More specifically, buoy data are retrieved from the CMEMS platform "European Marine Observation and Data Network" (EMODnet) [41].

Most of the buoy data (>98%) are available in hourly estimates. In addition to wind speed and direction information, both provided at anemometer heights (3 m), buoy measurements of required atmospheric and oceanic parameters such as temperatures and relative humidity are also provided. The use of quality control flags, available with data, allow the consistent assessment of reliable wind speed time series. To avoid the use of inhomogeneous (erroneous) data, not detected through the standard quality control process, or to reject correct data, each buoy time series is investigated individually, and proper selected statistical criteria are determined and applied. More specifically, for each month of the study period and each buoy, monthly-averaged buoy wind estimates, and the associated standard deviations, are calculated from the available buoy wind measurements. Buoy data exceeding three standard deviations monthly values are investigated individually. Hourly buoy winds are converted to 10 m neutral winds using COARE3.0 parameterizations [42].

Table 1 summarizes the main statistics allowing the characterization of wind speed at each buoy location (Fig. 2). As expected, the highest wind speed conditions are found at buoys located northwest of Spain, while the lowest winds are depicted near coast locations or in the Gulf of Cadiz. The three statistical conventional moments (standard deviation (STD), skewness (Skew), and kurtosis (Kur)) indicate that surface wind speed exhibit significant local characteristics. The latter would be further assessed through the estimation of temporal scale variability of wind speed from each buoy. Fig. 1 shows the autocorrelation of wind speed as a function time lag varying between 1 h and 36 h. It results that most of the wind speeds exhibit significant autocorrelation exceeding 0.80 at 95% confidence level, for time lag lower than 6 h. Therefore, the satellite surface wind analyses, used in this study, are estimated from remotely sensed data as 6-hourly averages at synoptic times (0000 UTC, 0006 UTC, 0012 UTC, 1800 UTC) over a gridded map of 0.125° in latitude and longitude.

2.2. WRF model wind estimates

WRF is a FLOSS (free libre open source software) model, fully compressible and non-hydrostatic, with a variety of capabilities that meets the needs of both operational forecasting and academic communities at a variety of spatial scales. It supports multiple dynamical cores, real-data and idealized simulations, data assimilation capabilities, a broad spectrum of physics and dynamic options as well as multiple types of nesting [43]. Details of the model setup are summarized in Table 2.

Within the context of this work, WRF version 3.9 was used to

Table 1
Buoy information including buoy WMO code, coordinates (latitude, longitude), period of data availability, mean 10 m wind speed (Mean), standard deviation (STD, skewness (Skew), kurtosis (Kur), 5% (P_{05}) and 95% (P_{95}) quartiles.

WMO Code	Latitude	Longitude	Period	Mean (m/s)	STD (m/s)	Skew	Kur	P_{05} (m/s)	P_{95} (m/s)
6200191	41.1500°N	9.5800°W	2010–2019	7.61	3.87	0.37	2.87	1.78	14.25
6200192	39.5100°N	9.6400°W	2009–2019	7.45	3.70	0.60	3.69	2.00	13.80
6200199	39.5600°N	9.2100°W	2010–2019	6.17	3.38	0.60	2.96	1.34	12.29
6201031	41.9011°N	8.8993°W	2010–2019	7.30	3.62	0.42	3.15	1.83	13.49
6201038	42.6295°N	8.7804°W	2007–2019	5.39	3.05	0.49	2.89	0.94	10.73
6201040	42.1719°N	8.9063°W	2008–2019	5.97	3.81	1.17	5.87	1.08	12.71
6201062	42.5500°N	8.9475°W	2011–2019	6.92	4.76	1.47	6.19	1.09	14.75
62025	43.7419°N	6.1679°W	1997–2019	6.03	3.64	0.67	3.07	1.07	12.71
62082	44.0896°N	7.6428°W	1996–2019	7.80	4.02	0.56	3.73	1.67	14.49
62083	43.4963°N	9.2134°W	1998–2019	7.81	4.16	0.29	2.53	1.39	14.96
62084	42.1225°N	9.4142°W	1998–2019	7.11	3.93	0.30	2.41	1.31	13.78
62085	36.4953°N	6.9650°W	1996–2019	6.30	3.33	0.55	3.07	1.43	12.24

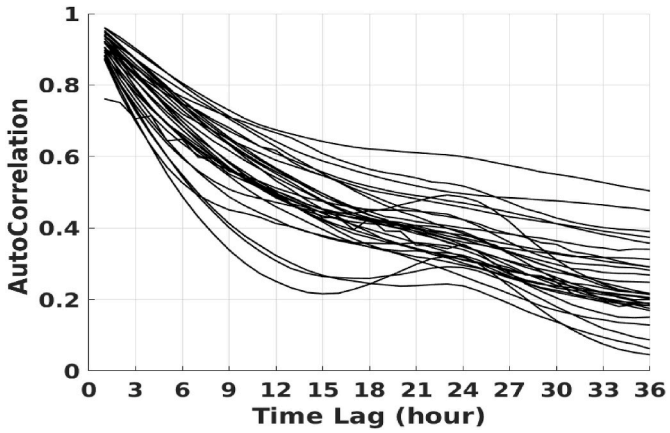

Fig. 1. Autocorrelations of wind speeds derived from buoys (Table 1) estimated from all available hourly measurements.

downscale the Era-Interim forecasts with 0.75° of horizontal resolution to a 9 km mesh grid on a 1:3 nesting configuration. The NWP model produces weather data with a 6-h temporal resolution and 47 vertical levels. The computational grid covers the Iberian Peninsula and part of the Atlantic Ocean. Fig. 2 illustrates the full operational setup of the WRF forecasting system along with the location of the marine buoys that supported the quantitative verification of the results.

2.3. Satellite retrieval of surface wind

The remotely sensed data used in this study is described in various papers (e.g. Refs. [44,45]). Satellite data used here are those available during the period 2004–2012. The reader may refer to the websites, shown in Table 3, providing details about instruments, wind processing, and relevant publications and reports. Briefly, the main sources of remotely sensed wind data are from scatterometers onboard QuikSCAT (1999–2009), Metop-A (2007 – present), and Metop-B (2012 – present). Ancillary remotely sensed data are derived from radiometers: Special Sensor Microwave Imager Sounder (SSMI/S) onboard the Defense Meteorological Satellite Program (DMSP) F16 (2003 – present) and F17 (2006 – present), and from WindSat onboard Coriolis satellite (2003 – present). 10 m wind speed and direction retrievals from SAR onboard Sentinel-1A (2014 – Present) and –1B (2016 – Present) are also of concern. They are mainly used for estimating the spatial variation at local scales [44].

Scatterometer and radiometer data used in this study are Level 2 (known as L2b product) wind retrievals available on wind vector cell (WVC) grid within the radar and radiometer ground swath, i.e., suitable areas (depending on radar/radiometer characteristics). Scatterometer and WindSat provide both wind speed and direction at 10 m height,

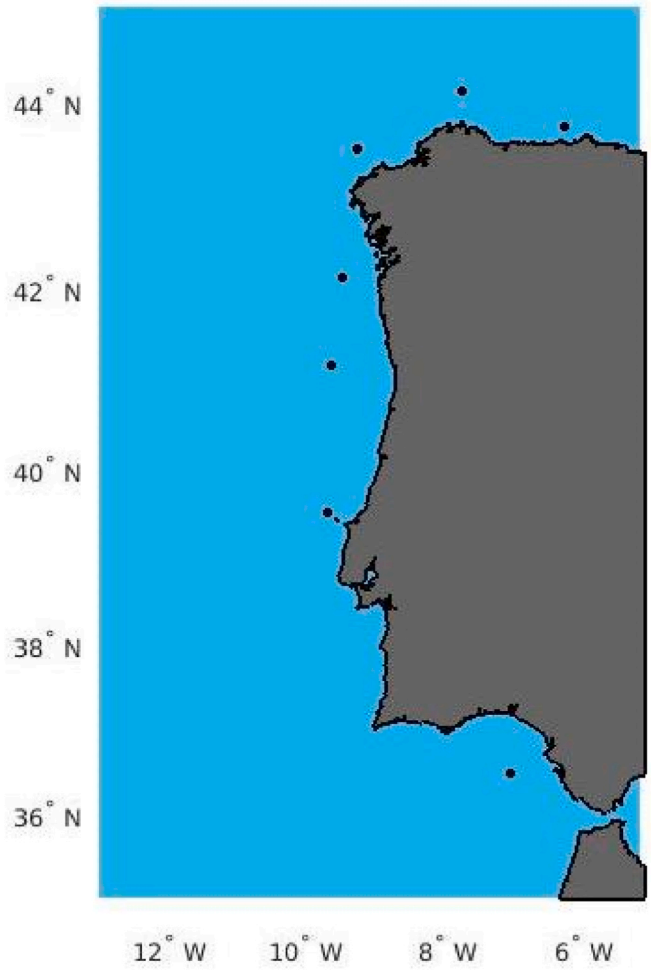

Fig. 2. WRF domain and location of the offshore buoys from EMODNET database.

while SSMI/S provide only 10 m wind speed. The WVC grid size varies among different wind products. QuikSCAT WVC grids are of 12.5 km × 12.5 km, while ASCAT WVC is of 25 km × 25 km until 2009, and of 12.5 km x 12.5. Scatterometer beams measure the normalized radar cross-section (NRCS), also known as backscatter coefficient (σ^0), from the wind-roughened sea surface, which is mainly a function of wind condition (speed and direction). Backscatter σ^0 data represent a dimensionless property of the surface, describing the ratio of the effective echoing area per unit area illuminated. Scatterometer wind retrievals are obtained from σ^0 measurements through an inversion procedure

Table 2
WRF system configuration and parameterization options.

Horizontal Resolution (km)	9
Temporal resolution (hours)	6
Grid Dimension	96 × 148
Vertical Grid dimension	47 eta levels
Radiation	CAM scheme for both short and long wave radiation
PBL Physics	Yonsei University scheme
Land Surface	Unified Noah Land Surface Model
Microphysics	WRF Single-Moment 6-class scheme
Cumulus	Kain-Fritsch scheme

Table 3
Relevant websites providing information about radars and radiometers used in this study.

Satellite	Period	Website
QuikSCAT	1999–2009	https://podaac.jpl.nasa.gov/dataset/QSCAT_LEVEL_2B_OWV_COMP_12,
ASCAT	2006 – Present	projects.knmi.nl/scatterometer/ascat_osi_12_prod
SSMI/S F16	2003 - Present	http://data.remss.com/ssmi/f16/bmaps_v07/
SSMI/S F17	2007 - Present	http://data.remss.com/ssmi/f17/bmaps_v07/
WindSat	2003 - Present	http://data.remss.com/windsat/bmaps_v07.0.1/
Sentinel SAR	2014 - Present	https://sentinel.esa.int/web/sentinel/missions/sentinel-1/data-products

based on the use of Geophysical Model Functions (GMF). Scatterometer wind retrievals are provided over swaths of 1800 km (QuikSCAT), and 2 × 600 km (ASCAT). The links shown in Table 3 provide technical details related to scatterometer wind processing. References such as [42–44] provide results related to the accuracy of scatterometer wind retrievals.

The ancillary remotely sensed wind data used in this study are retrieved from the special sensor microwave imager (SSM/I) and sounder (SSMI/S) brightness temperature measurements (T_B). Only surface wind speed at 10 m height can be derived from SSMI and SSMI/S T_B based on the use of an empirical model fitting the relationship between surface wind speed and T_B through the radiative transfer equation (RTE). They are provided by a remote sensing system (RSS) [46]. SSM/I and SSMI/S wind data are available over swath (1400 km width) at wind cell of 0.25° in latitude and longitude over global oceans.

Sentinel-1A and –1B SAR wind speed and direction retrievals, used in this study, are known as level 2 ocean (L2OCN) products, acquired in interferometric wide (IW) swath mode. Data are available over a swath of 250 widths, with a moderate geometric resolution of 5 m × 20 m. Details about SAR winds and the related accuracy are available in the literature [44].

Several publications provide useful information related to improving the accuracy of the remotely sensed winds (see for instance Ref. [47]). For this study, the accuracy, at the regional scale, of the remotely sensed winds is briefly assessed through comprehensive comparisons with buoy measurements used in this study. To achieve the comparison, buoy and satellite wind retrievals are collocated based on the spatial and temporal criteria, 25 km and 1 h, respectively. Table 4 summarizes some statistical parameters aiming at the characterization of the comparisons of buoy and satellite retrieval wind speeds, zonal components, and meridional components. The resulting statistical parameters shown in Table 4 are also required for the calculation of blended winds (see hereafter).

The resulting statistics (Table 4) are determined assuming that buoy and satellite winds are both non-error-free. Only those obtained for scatterometers QuikSCAT and ASCAT are shown. Both are similar to those obtained from scatterometer accuracy determination based on the use of buoy networks such as National Data Buoy Centre (NDBC) and Météo-France and U.K. Met Office buoys [48]. Biases are small, RMS

Table 4
Comparison of statistical parameters of collocated 10 m wind speed, zonal, and meridional components from buoys and QuikSCAT, ASCAT retrievals, and WRF model analyses for 2004–2012. Bias is defined as the mean difference between buoy and product winds (in this order). RMS, b_s, a_s, and ρ, indicate root mean difference, regression coefficients (slope and intercept), and scalar correlation coefficient, respectively. Length is the number of collocated buoy and satellite wind data. Similar statistics are also shown for Sentinel-1a SAR IW winds. The former is estimated from buoy and SAR collocated data for 2015–2018.

	Wind Speed					
	Length	Bias(m/s)	RMS(m/s)	b_s	a_s (m/s)	ρ
QuikSCAT	29911	−0.17	1.39	0.90	0.72	0.95
ASCAT	18252	0.06	1.27	0.91	0.57	0.95
SAR	3887	0.45	1.65	0.86	0.49	0.91
Zonal wind component						
QuikSCAT	29390	0.21	2.54	1.20	−0.20	0.92
ASCAT	18115	0.03	1.66	1.15	−0.02	0.96
SAR	3719	0.13	1.83	1.07	−0.12	0.93
Meridional wind component						
QuikSCAT	29572	−0.50	2.21	1.14	0.38	0.91
ASCAT	18080	−0.13	1.68	1.15	−0.02	0.96
SAR	3787	−0.42	2.04	1.05	0.37	0.92

wind speed differences do not exceed 1.40 m/s, and correlation exceeds 0.90 at 95% confidence. RMS differences of QuikSCAT zonal and meridional wind components exceed 2 m/s, while those estimated for ASCAT are about 1.70 m/s. It results from the difference in collocated buoy/QuikSCAT and buoy/ASCAT low wind speed (<5 m/s) distributions. They account for almost 27%, and 22% of the total length of collocated data, respectively. Excluding wind speeds lower than 5 m/s, lead to similar statistics for QuikSCAT and ASCAT wind components (not shown).

Table 4 also shows statistics aiming at the characterization of the comparison between a buoy and SAR IW winds. They are only required for the determination, from SAR IW retrievals, of the spatial structures of surface wind speed, zonal, meridional wind components along the area of interest (see section 2.4). Buoy and SAR IW agree well. However, SAR IW wind speed tends to be underestimated compared to buoy measurements [49]. Briefly, it relies on GMF used for retrieving wind speed and direction from the SAR backscatter coefficient.

2.4. Blended WRF and satellite wind fields

The method aiming at the determination of regular space and time surface wind fields, named surface wind analyses, over the oceanic area of interest, from remotely sensed observations, is described in previous papers (e.g. Ref. [49]). It is an objective method based on the kriging technique with the external drift method as described in the aforementioned reference. External drift is from the WRF model. Briefly, the scatterometer and radiometer winds are used to estimate 6-hourly averaged wind speed and direction over all grid cells of 0.125° in latitude and longitude (except grid cells over land).

The contribution of each remotely sensed data requires knowledge of the associated weight. The latter accounts for the spatial and temporal separations of the analysis. Weight determination requires the knowledge of the spatial and temporal variability function (named variogram) of wind speed, zonal, and meridional components. Variograms illustrate the spatial and temporal scales of the variable, which are highly related to the space and time covariance functions. In practice, the variogram is determined as a parametric function, requiring the determination of three parameters. Two parameters, called variogram spatial and temporal ranges, indicate respectively the spatial and temporal lags beyond where no significant spatial and temporal correlation between wind variables are drawn. The third parameter (called sill) is the variogram value associated with the variogram ranges.

Fig. 3 shows the spatial scales (in km) of wind speed of the related wind components. They are determined from SAR IW retrievals based on the use of the method described in Ref. [45]. Briefly, for each hour of the day and each point on a 0.125° × 0.125° grid, SAR-based wind covariances are estimated as a function of distance δh for 1 km$\leq \delta h \geq$ 300 km at 5 km steps. The hourly statistics is estimated only if the sampling length of SAR retrievals is significant ($\geq$30). Space distribution of the spatial scales reflects the nature of local air–sea-land interactions and generally aligns with local topography. The presence of sharp landmasses (such as capes) would introduce apparent inhomogeneities to spatial scale maps. Local air–sea-land interactions are also reflected in the spatial distribution of wind scale patterns that tend to be aligned with regional coastal configuration and topography.

Wind speed (Fig. 3a) exhibits small spatial scales, laying between 10 km and 30 km, over coastal areas (<100 km of coastlines), while over offshore areas, these scales are mostly higher than 50 km. As expected, regarding spatial wind patterns, the coastal wind speed scale exhibits a significant zonal pattern. Similar results are found for the zonal wind component (Fig. 3b) and meridional wind component (Fig. 3c). However, their spatial scales are larger than those found for wind speed and generally exceed 30 km, except at a few locations.

The determination of the variogram temporal range is based on the use of the results drawn from the buoy temporal autocorrelation behaviours (Fig. 1). The former indicates that the wind temporal scale would be lower than 12 h.

The resulting variograms are then used as inputs of the objective method components aiming at the determination of regional satellite wind analyses at synoptic times. The latter is also referred to as blended satellite winds or 6-hourly satellite wind analyses. An example of these wind analyses is shown in Fig. 4. It shows four consecutive 6-hourly analyses of February 27, 2010. It assesses the spatial and temporal variability of wind speed as well as wind direction, associated with

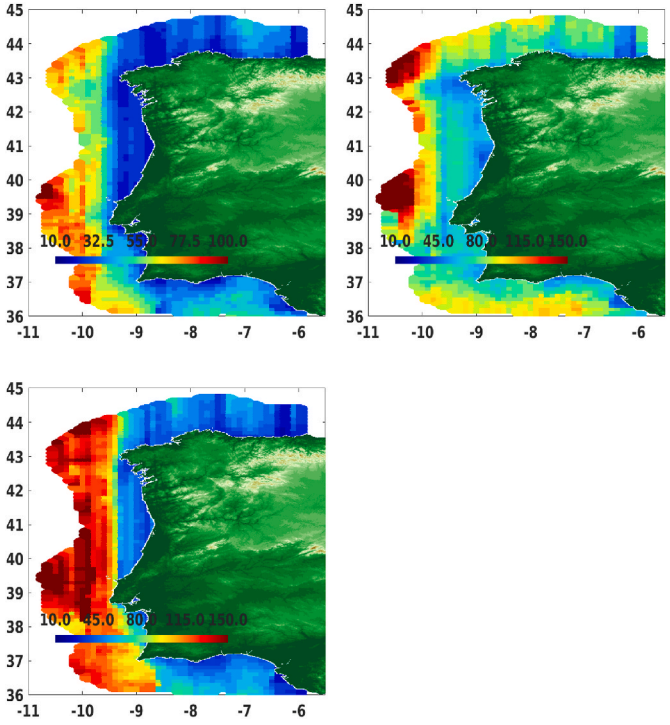

Fig. 3. Spatial wind patterns of a) wind speed (m/s), b) zonal wind component (m/s), and c) meridional wind component (m/s), estimated from Sentinel SAR wind retrievals. They are determined at each grid cell (0.125° × 0.125°) off Portugal and Spain's Atlantic coasts. The x-axis and y-axis represent the longitude and latitude of the domain. The colour shows the spatial scale value (in km).

southeast-northeast high wind condition development.

Fig. 5 shows an example of the differences across the two datasets, the WRF and blended winds, for the strong wind episode occurring on February 27th. It can be seen that the WRF model can reproduce the wind pattern generally well. Areas of increased wind speed in the northwest corner are visible in both maps although it is clear that WRF underestimates high wind speeds between the 37° and 43° parallels. The general tendency for WRF to underpredict strong winds is well known and has previously been discussed [39]. In contrast, across the area of the highest concentration of strong winds, at the northwest corner of Galicia, WRF overestimates the maximum observed winds. This was confirmed by comparison with buoy measurements in that area not presented in this section The use of the blended product allows correcting the model bias further improving the accurate reproduction of the local meteorological phenomena.

The resulting satellite 6-hourly analyses are first compared to remotely sensed wind data. It assesses the ability of satellite analyses to restore the observed surface wind characteristics. To achieve such comparisons, satellite wind analyses and WRF wind estimates are collocated in space and time with satellite observations. The collocation spatial and temporal criteria are 25 km, and 3 h, respectively. Fig. 6 shows the time series of statistical parameters (mean difference (bias), the standard deviation of the difference, and correlation), estimated at a regional scale, aiming the characterization of the comparison between satellite wind speed observations and, on one hand, satellite analyses, and on other hand WRF estimates. It is concluded that satellite wind analyses improve the results of the comparisons. Indeed, Bias as STD is reduced and correlation increases, compared to results found for WRF.

Nine years (2004–2012) of satellite wind analyses are calculated. Their accuracy is determined through comprehensive comparisons with 6-hourly averaged buoy (Table 1) wind speed and direction. The latter is estimated from valid 10 m hourly wind data available within 3 h of synoptic times. Only 6-hourly buoy data estimated at least with 3 hourly measurements are selected for comparison purposes. Buoy and satellite 6-hourly winds available at the same synoptic times and located within 12.5 km of each other, are selected as collocated data, and used for the determination of satellite analysis accuracy. A similar procedure is used for collocating in space and time buoy and WRF winds.

Fig. 7 shows a comparison between buoy and satellite (left column panels) and between buoys and WRF (right column panels). Both WRF and satellite exhibit good agreement with buoy data. However, satellite analysis improves the comparisons, especially for wind speed (Fig. 7 a and b). The scatter of the satellite wind speed analysis is reduced for almost all wind speed ranges. More specifically, the RMS of the difference between buoy and satellite, and between buoy and WRF are 1.71 m/s, and 1.97 m/s, respectively. Although satellite zonal (Fig. 7 c)) and meridional (Fig. 7 e)) wind components exhibit better comparison results, compared to WRF results (Fig. 7 d) and f)), the improvements are quite limited. For instance, the RMS difference values of the zonal component are 2.06 m/s and 2.19 m/s for satellite and WRF, respectively (Fig. 8).

It is worth mentioning that the performance metrics presented here are in-line with those published in similar studies. Other authors compared WRF simulations against the same network of buoys used in this work, obtaining analogous results for the same statistical scores [36]. Similarly, the authors in another study obtained analogous RMSE values in comparisons of WRF against 8 mast and lidar sites across northern Europe [50]. This is an important result since these were the results of the validation that preceded the creation of the New European Wind Atlas. Still, WRF model has been tuned and tested in the region that motivated this study turning it into a better choice for on-site resource assessment.

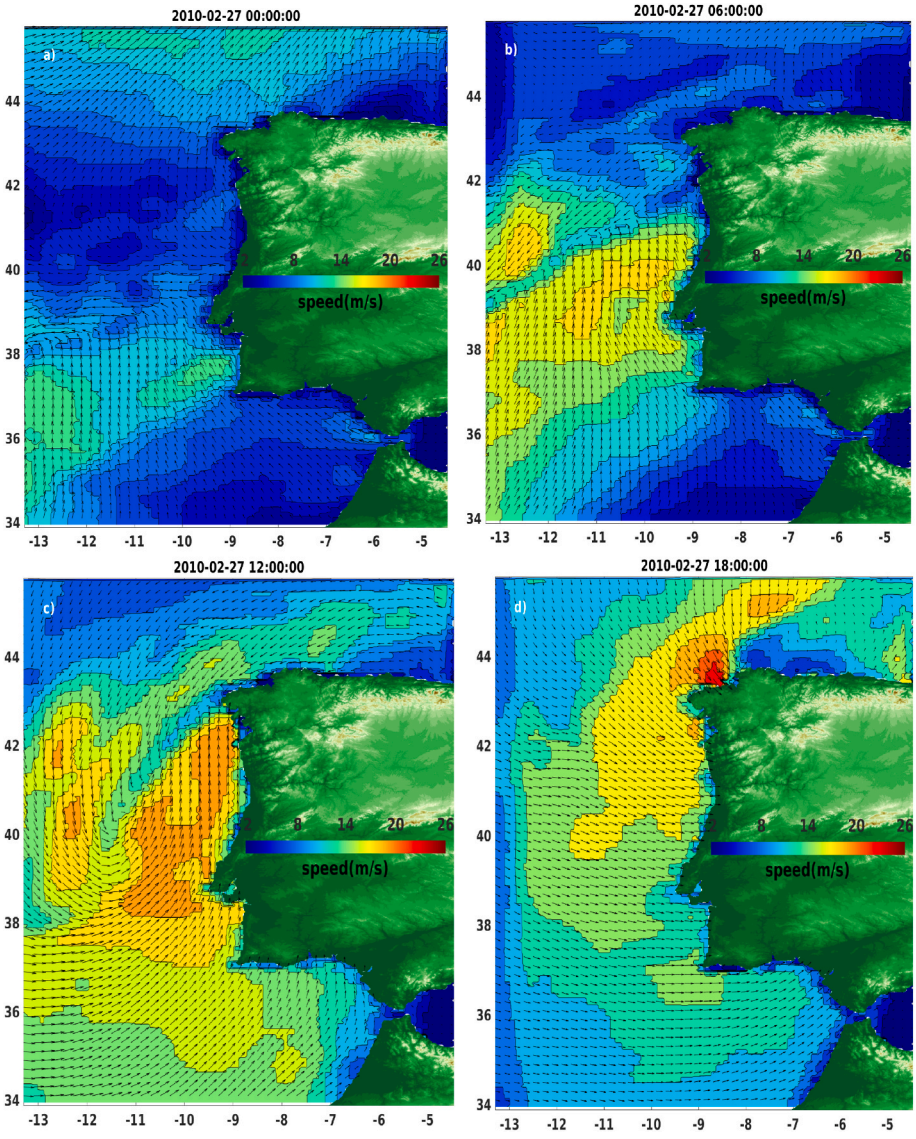

Fig. 4. Examples of four consecutive 10 m blended satellite wind analyses occurring on February 27, 2010 at the synoptic time a)00 h:00, b)06 h:00, c)12 h:00, and d)18 h:00 UTC. The x-axis and y-axis represent the longitude and latitude of the domain. Colour indicates wind speed values, while the black arrows indicate wind direction.

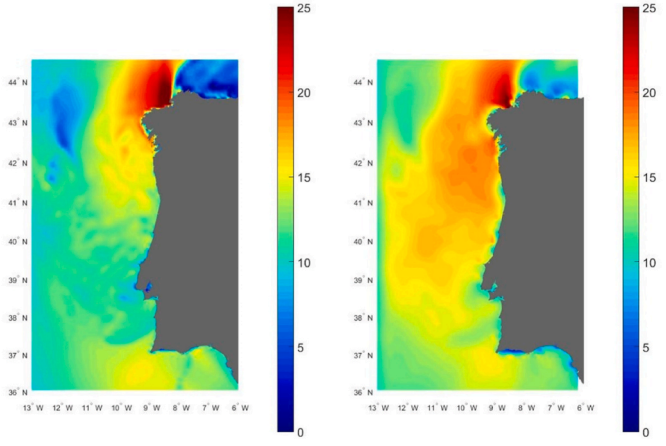

Fig. 5. Example of the difference between WRF 10 m wind speed (left) and blended wind maps for the high wind episode occurring on February 27, 2010 at synoptic time 18:00.

3. Validation of the dataset

3.1. Wind speed

In this section, the spatial and temporal wind patterns are analysed in more detail using the blended winds described in the previous section. To gain further insight into the spatial pattern of the mean wind speed, a wind map is drawn and displayed in Fig. 9 (left panel). As it is observed, two main characteristic patterns are evident from the colour distribution analysis. The wind speed is higher in the northern regions, most particularly in the northwest corner of the Iberian Peninsula, where wind speed is above 8.5 m/s on average.

This region of Galicia is affected by strong west winds that come from the Atlantic low-pressure systems. As expected, winds rapidly increase with the distance to the coast varying between 5 and 6 m/s along the western coast and rapidly increasing up to 8.5 m/s in the northern regions. In the south, the lowest wind speeds occur, with magnitudes of around 4–5.5 m/s near the coast though they still represent attractive conditions for wind projects. Overall, winds vary between 6 and 7.5 m/s in the west side of the Iberian Peninsula, most affected by western

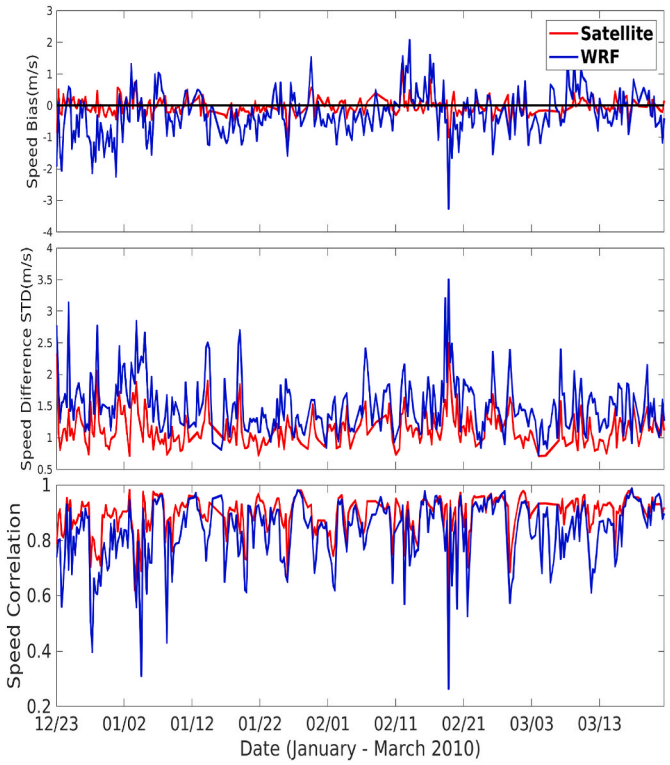

Fig. 6. Time series (January 1st - March 31st, 2010) of statistical parameters (mean (bias) (panel on top) and standard deviation (STD) (middle) wind speed difference, and the related correlation coefficient (in bottom)) characterizing the comparisons between satellite wind speed observations and analyses (shown in red colour), and between satellite wind speed observations and WRF estimates (in blue colour).

Atlantic winds, indicating good overall conditions for building wind parks taking into account the average water depth and distance to shore of offshore wind farms [51].

In addition to the annual means, extreme winds are calculated using the statistical percentile procedure (Fig. 9, right panel). In this paper, the threshold chosen to define the extremes was the 99th percentile. The map at the upper percentile level (right panel of Fig. 9) shows that the lowest extreme winds occur in the south, not exceeding 14 m/s on average. This is also valid near the coast throughout most of the domain, though rapidly increasing up to 17 m/s in the northmost regions and with the distance from the coast. This is suitable for most wind turbines which have a typically rated speed of 11–17 m/s and cut off speed of 25 m/s [52,53].

3.2. Annual wind variability

To access the inter-annual variability, Fig. 10 shows the normalized wind speed from 2004 to 2012. The deviations from the mean are calculated by dividing each year's average wind speed records by long-term mean throughout the 9 years $u = U/\overline{U}$. These numbers allow analysing the variability for the 9 years and to estimate the deviations from the long term mean value during that period.

The results show that the annual wind speed ranges from a low of 85–90% of the 9-yearly mean wind speed to a high of 125% of the average intensity. An increasing trend is noticed throughout 2010 though preceded by lower the intensity year of 2009. According to the wind analysis, the years 2008 and 2010 show the higher average intensity up to nearly 115% of the medium-term mean contrasting with the years of 2004 and 2007 that show lower intensity winds. For the year 2010 in particular, the distinct pattern is likely related to the strong signature of North Atlantic Oscillation [54]. These maps give a general overview of the spatial and temporal patterns of the wind in the selected region, however, a thorough analysis must be done in specific regions for wind turbine implementation.

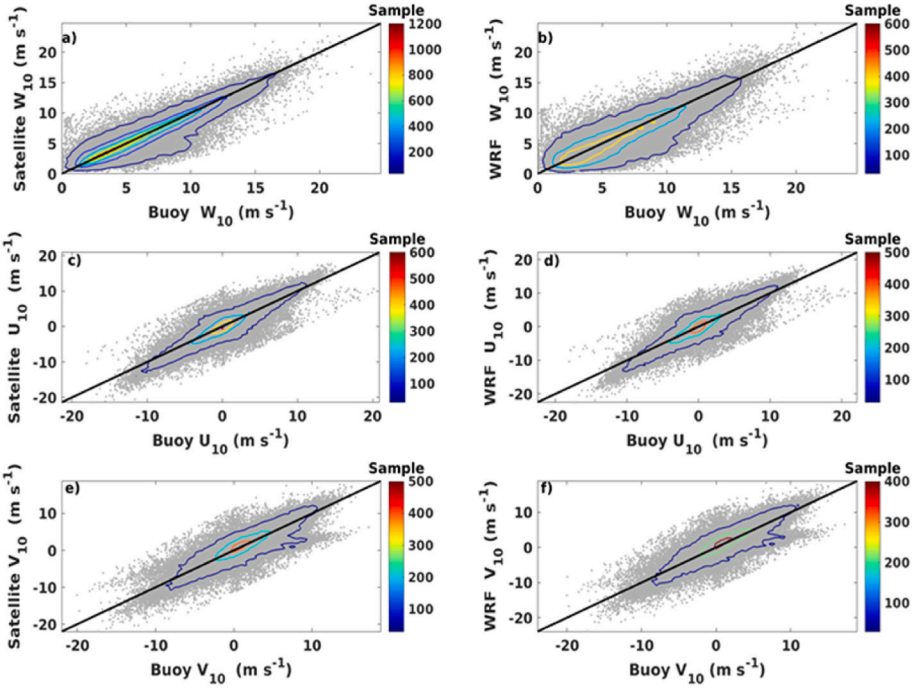

Fig. 7. Comparison of 6-hourly buoy and satellite analyses (left column), and between buoys and WRF (right column). Panels in the top (a) and b)), middle (c) and d)), and bottom e) and f)) show wind speed, zonal, and meridional comparisons, respectively. Coloured contours indicate the sampling length of collocated data associated with wind bins of 0.50 m/s width. Only contours associated with sampling length exceeding 30 are shown.

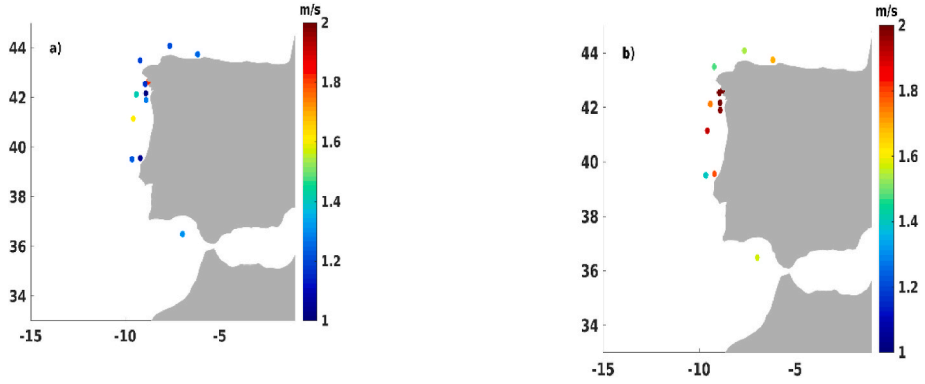

Fig. 8. Root mean square differences (RMSD) between buoy and satellite (a), and between buoys and WRF wind speed (b), shown at buoy locations.

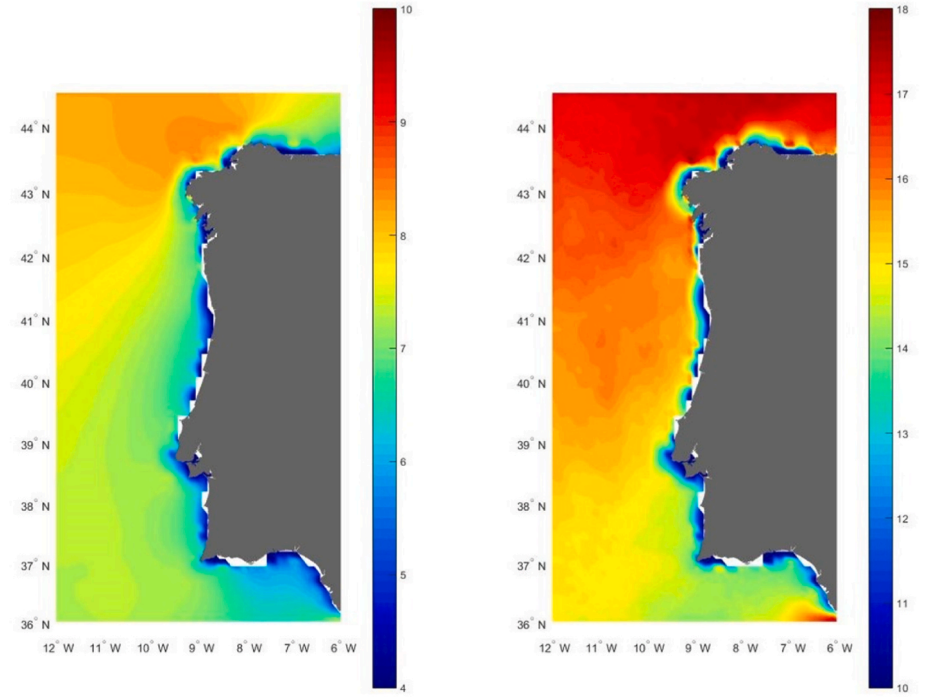

Fig. 9. Annual average 10 m blended wind speed (m/s) for the 9-year period (left) and 99th percentile (right).

3.3. Seasonal wind variability

The seasonal distribution of winds for the study area is shown in Fig. 11. As expected, the winter represents the most energetic season with winds of greater magnitude occurring more frequently, especially above the 7 m/s threshold and exceeding 9 m/s in the northern regions. Conversely, lower magnitude winds occur more frequently in the spring and summer even though the difference is more noticeable in the northwest corner of the domain. Along the coast, winds still exceed on average 6 m/s which still represents attractive conditions. This is due to the strong winds that occur during summer in Portugal, created by a thermal low over the Iberian Peninsula and the Azores high-pressure system [55]. These blow mostly from North-Northeast directions and contribute to the potential for wind exploitation during these months.

Fig. 12 shows the spatial distribution of winds exceeding the 99th percentile. The winds exhibit similar spatial characteristics to the average wind displayed in Fig. 11. Overall, extreme winds range from 11 to 19 m/s over the selected domain throughout the year. All seasons have their largest winds in the northwest corner of the domain, in agreement with the median wind maps. Similarly, summer is the period with the lowest magnitude winds. It is also interesting to notice that for the winter and fall seasons, the spatial distribution of the extreme wind differs in how it compares with the median wind pattern. Although the winds are stronger on average during the winter season between the 37 and 41° parallels, fall months are subject to larger magnitude extreme winds in this subsection of the domain.

4. Wind energy

One of the potential benefits of an accurate wind product is an accurate estimation of wind energy. The energy resources at selected regions of interest have been determined using the blended wind product. The wind power density (WPD) is calculated over the entire area and further in detail for the three proposed locations for wind turbine implementation. The wind power density is calculated considering the wind speed frequency of occurrence in 1 m/s intervals, using the following expression:

$$WPD = \frac{1}{2}\rho v^3 \quad (6)$$

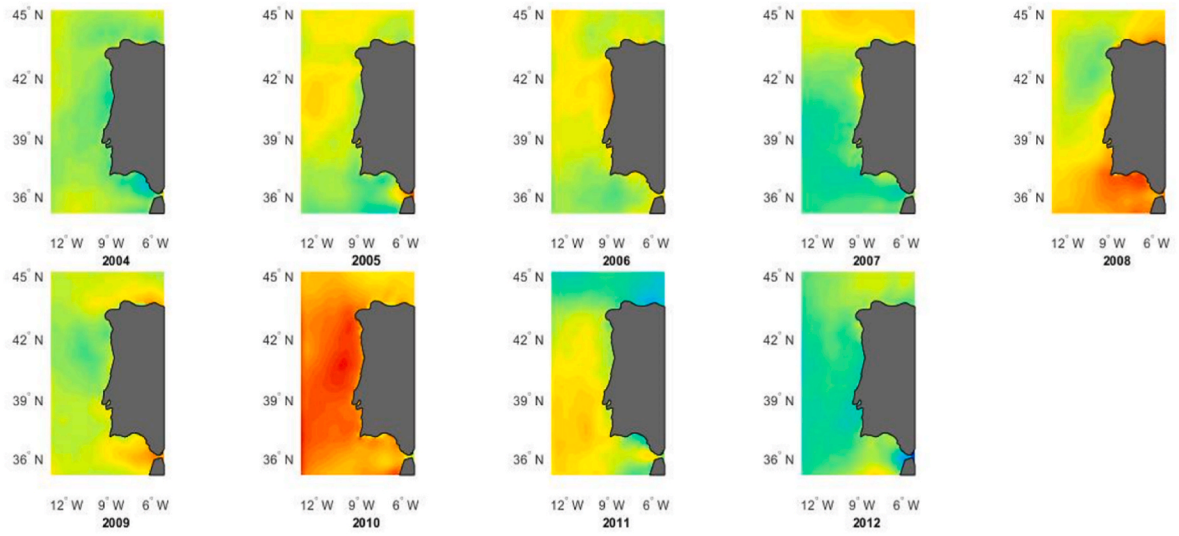

Fig. 10. Normalized wind speed (m/s) for 2004–2012. The deviations from the mean are calculated by dividing each year average wind speed records by the 9-yearly mean wind speed.$u = U/\overline{U}$*100

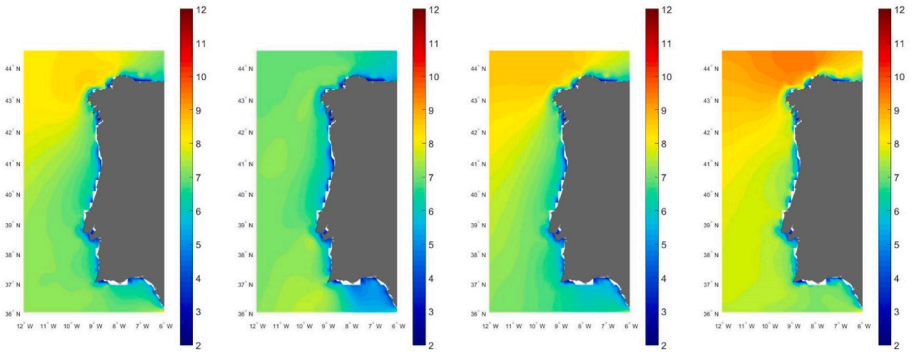

Fig. 11. Wind speed seasonal variations (m/s). From left to right (spring, summer, fall, winter).

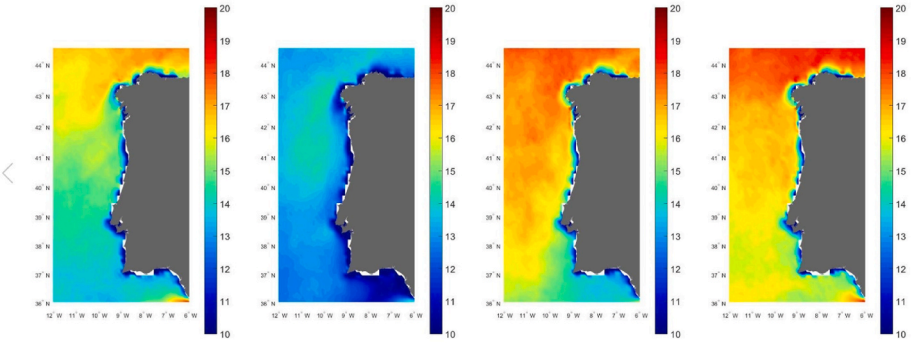

Fig. 12. 99th percentile wind speed (m/s). From left to right (spring, summer, fall, winter).

where the air density ρ (kg/m^3) is taken as 1.225 kg/m^3.

From the seven wind power classes defined [56], class 3 and above are considered suitable for most wind power projects. This corresponds to a WPD of 150/200 W/m^2 at 10 m height or the equivalent 5.1/5.6 m/s mean wind speed. Fig. 13 shows the spatial pattern of the wind power density obtained from the satellite analyses. The northern region denotes the highest potential while the southern areas have more modest values available for exploitation. Still, there is an overall high amount of energy along the entire coast with great dependence upon the distance to the coast. Nearly 350–400 W/m^2 (class 6) are available in average for extraction offshore the north and central coast and 250–300 W/m^2.

The pronounced seasonal variations of the energy density in the Iberian Peninsula offshore area are depicted in Fig. 14. Three sites are marked to identify the most energetic region across the country. Porto, Ericeira and Albufeira are some of the potential sites, a choice that was based on a preliminary inspection of physical and environmental limitations among other constraints [57].

The maps illustrate how the winds are maximum during winter months and less intense during the rest of the year in agreement with what was presented in subsection 3.4. Summer is the least energetic

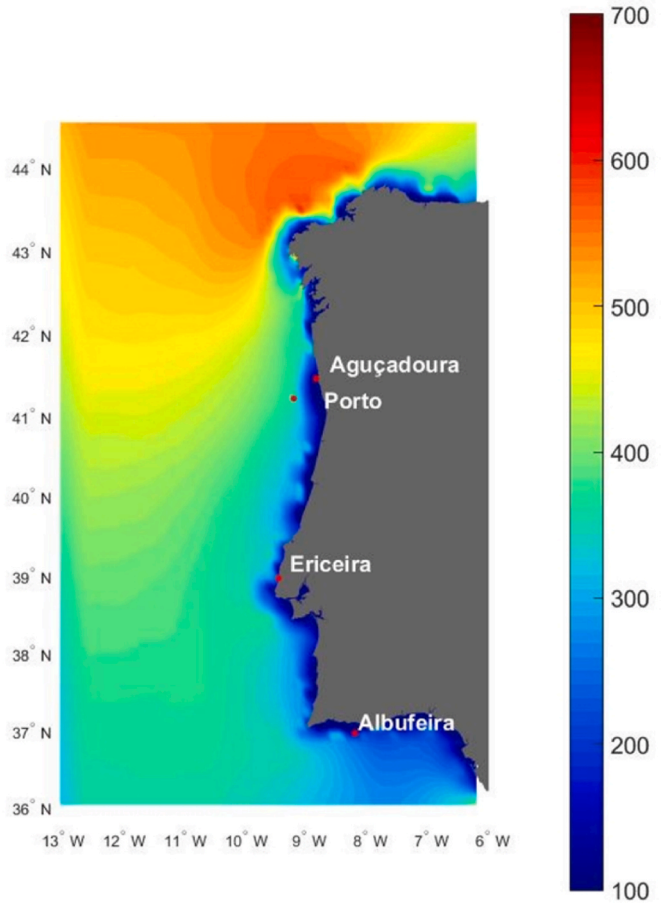

Fig. 13. Average Wind power density (W/m^2) in the Iberian Peninsula coast from 2004 to 2012; winds obtained from the satellite analyses.

season, but the potential progressively increases until it reaches its maximum value during the winter season. In terms of overall potential, the values vary around 300–600 W/m^2 during the winter season decreasing to 100–300 W/m^2 during the summer. It is interesting to notice that during summer the spatial variability is remarkably decreased when compared with the other seasons. Still, even during the least energetic seasons, the observed potential corresponds to a wind class 5.

Figs. 15 and 16 show the 10 m wind speed time series for two wind energy test sites. The two datasets are compared: wind data obtained from WRF model and the new blended winds. Additionally, the results obtained from wind speed derived from the new European wind atlas is also summarized in Table 5. Figs. 15 and 16 show a generally good agreement between the two datasets as expected though WRF derived winds are consistently higher throughout the year which can lead to an overestimation of the available resource at a particular site. In addition, an inspection of Table 5, shows that even a small difference in the average wind speed can translate into power density differences of roughly 200 W/m^2 annually. The opposite is also true.

As an example, at Albufeira, despite the similar average wind power density estimated for the year 2012, the average wind speed differs by only 1 m/s. But oppositely, at Aguçadoura, 1.6 m/s difference in the average wind translate into nearly 200 W/m^2 of available power while 0.3 m/s difference from the wind Atlas dataset derived wind, in turn, would mean an additional 250 W/m^2 yearly. Looking at the wind Atlas annual values we can see they are quite similar even though the two regions have considerable differences in the actual wind resource. To give an example of the implications of such differences, at Albufeira considering the WRF results, a wind turbine with a cut-in wind speed of 4 m/s would operate 354 days per year while using the blended winds the forecast is 339 working days. This has strong implications, especially when assessing a realistic maximum yield of offshore wind as the numbers will dictate investment needs and designing strategies to maximize the net energy flux. If we take into account the validation of the blended winds, and consider them accurate, this will affect the wind energy projections. Still, a comparison with observations such as buoy or

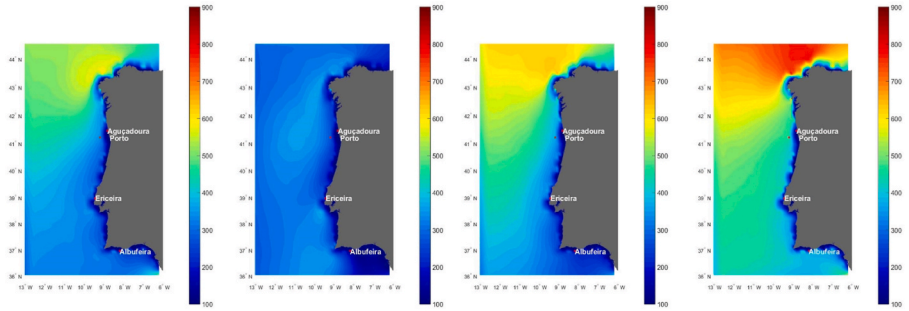

Fig. 14. Wind power density seasonal variations (W/m^2). From left to right (spring, summer, fall, winter).

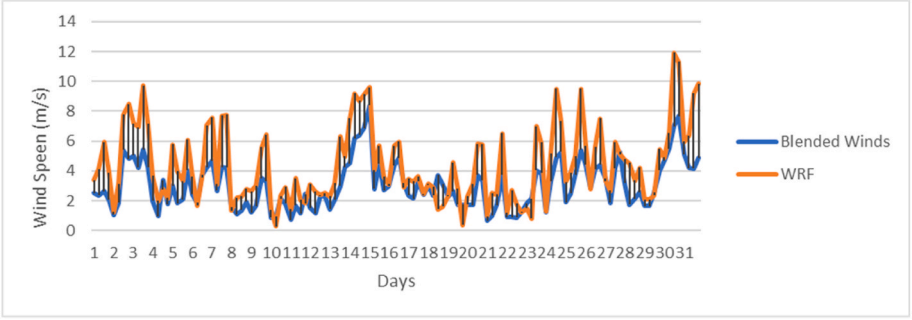

Fig. 15. 10 m wind speed (m/s) offshore Aguçadoura during the month of August of 2012.

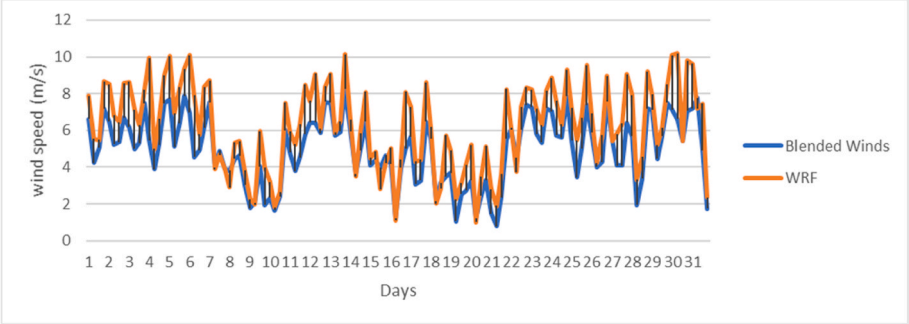

Fig. 16. 10 m wind speed (m/s) offshore Albufeira during August of 2012.

Table 5
Mean Wind speed and power density values for two selected wind energy test sites.

Source	Area	Aguçadoura	Albufeira
WRF	Wind Speed (m/s)	4.10	6.34
	WPD (W/m^2)	243	278
Blended data	Wind Speed (m/s)	5.74	5,31
	WPD (W/m^2)	459	285
Wind Atlas	Wind Speed (m/s)	5.48	5.90
	WPD (W/m^2)	214	220

mast data would be of utmost importance in the initial stages of a wind project.

5. Discussion and conclusions

The main goal of the work presented in this paper is to develop a new wind product capable of addressing the main limitations of two of the most commonly used methods for generating the existing wind datasets: satellite data and numerical weather prediction models. For this purpose, wind data from scatterometers, radiometers, Synthetic-aperture radar and a wind forecasting model are combined and the potential improvements of the new analyses were assessed by comparison with a network of offshore buoys moored along the Iberian Peninsula coast. The results show that blended winds improve the agreement with wind observations, reducing the bias and improving every statistical score evaluated. The scatter of the satellite wind speed analysis is reduced for almost all wind speed ranges further reducing the magnitude of the wind power estimation error.

Several wind atlases are already publicly available and have been used for site selection and for designing energy harnessing systems worldwide. These use data mainly from reanalysis datasets or satellite information. However, these tools can still introduce uncertainty from its main components: mesoscale and microscale modelling. Similarly, several studies have already provided reasonably accurate estimates of the wind speed and energy resources in the region that concerns this work by using numerical models. The main strength of the dataset presented is the fact that since the WRF model has been used in this area in several studies, the combination of physical parameterizations used here with satellite data aims at providing better results than the ones we would obtain from the existing reanalysis and wind maps.

The main strength of this research is that it uses the existing knowledge obtained from the multiple sensitivity and assessment studies in this geographical area in combination with skilful satellite data to create improved wind information for the Portuguese coast.

The second part of this work presents an example of an application of this new wind dataset: an improved regional wind atlas to identify suitable areas for wind parks.

To give an example of the applications of this product a spatial and temporal analysis of the wind patterns is also carried out. The results show that a significant percentage of the winds vary from 5.5 to 8.5 m/s and despite some seasonal and interannual variations, the conditions are very attractive for new wind projects. As expected from a location in the northern hemisphere, winter presents a more energetic season with stronger winds over the entire domain and a higher probability of occurrence of extreme events.

Though locations close to the shoreline are still economically profitable, it is shown that the wind rapidly increases with the distance to the coast. Analyzing the energy projections, it can be concluded that northern regions concentrate most of the energy consistently throughout the seasons. Overall, the energy hot spots are located in the central and northern regions with the energy attaining its maximum at the northwest corner of the Peninsula. Still, the wind power class is above the threshold of three for all seasons and years which confirms the economic feasibility at this preliminary assessment stage. At Porto and Ericeira, two promising areas to harness energy in its vicinity, around 350–400 W/m^2 are available for extraction, on average, during the 2004–2012 period. When comparing the results against the data from wind atlas, differences up to 200 W/m^2 from the estimated wind power can be detected, which provides additional support that the choice of the dataset is of utmost importance for site selection.

Looking into the results provided by the newly generated wind maps shows that the entire area is promising for renewable energies, but a high wind energy site alone is not the only requirement for building wind parks. The next step would be combining the results of this study with the existing knowledge on the limitations imposed by physical and environmental constraints such as distance to shore, biodiversity protection, shipping routes, military areas, human activity, oil and gas exploration and tourist zones [58].

Finally, the new blended winds can be used to generate time series for promising sites around the world along with the estimation of the maximum wind energy yield for use in renewable energy system models. The techniques described in this paper can be applied to any test site and help correct numerical model bias, improving future wind integration studies.

CRediT authorship contribution statement

Nadia Salvação: Methodology, Formal analysis, Writing – original draft, Visualization. **Abderrahim Bentamy:** Methodology, Formal analysis, Writing – original draft, Visualization. **C. Guedes Soares:** Conceptualization, Writing – review & editing, Supervision.

Declaration of competing interest

The authors declare that they have no known competing financial interests or personal relationships that could have appeared to influence the work reported in this paper.

Acknowledgements

This work was conducted within the ARCWIND project–Adaptation and implementation of floating wind energy conversion technology for the Atlantic region (EAPA 344/2016), which is co-financed by the European Regional Development Fund through the Interreg Atlantic Area Programme. This work contributes to the Strategic Research Plan of the Centre for Marine Technology and Ocean Engineering (CENTEC), which is financed by the Portuguese Foundation for Science and Technology (Fundação para a Ciência e Tecnologia - FCT) under contract UIDB/UIDP/00134/2020.

References

[1] E.J. Palin, A.A. Scaife, E. Wallace, E.C.D. Pope, A. Arribas, A. Brookshaw, Skillful seasonal forecasts of winter disruption to the U.K. Transport system, J. Appl. Meteorol. Climatol. 55 (2) (2016) 325–344.
[2] P.E. Bett, H.E. Thornton, J.F. Lockwood, A.A. Scaife, N. Golding, C. Hewitt, R. Zhu, P.Q. Zhang, C.F. Li, Skill and reliability of seasonal forecasts for the Chinese energy sector, J. Appl. Meteorol. Climatol. 56 (11) (2017) 3099–3114.
[3] H.M. Diaz, C. Guedes Soares, Review of the current status, technology and future trends of offshore wind farms, Ocean. Eng. 209 (2020), 107381.
[4] L. Castro-Santos, E. Martins, C. Guedes Soares, Cost assessment methodology for combined wind and wave floating offshore renewable energy systems, Renew. Energy 97 (2016) 866–880.
[5] L. Castro-Santos, D. Silva, A.R. Bento, N. Salvação, C. Guedes Soares, Economic feasibility of floating offshore wind farms in Portugal, Ocean. Eng. 207 (2020), 107393.
[6] L. Castro-Santos, A.R. Bento, D. Silva, N. Salvação, C. Guedes Soares, Economic feasibility of floating offshore wind farms in the north of Spain, J. Mar. Sci. Eng. 8 (1) (2020) 58–76.
[7] M. Christoforaki, T. Tsoutsos, Sustainable Siting of an Offshore Wind Park a Case in Chania, Crete, vol. 109, Renewable Energy, 2017, pp. 624–633.
[8] H.M. Diaz, C. Guedes Soares, An integrated GIS approach for site selection of floating offshore wind farms in the Atlantic Continental European coastline, Renew. Sustain. Energy Rev. 134 (2020), 110328.
[9] H.M. Diaz, R.B. Fonseca, C. Guedes Soares, Site selection process for floating offshore wind farms in Madeira Islands, in: C. Guedes Soares (Ed.), Advances in Renewable Energies Offshore, Taylor & Francis, 2019, pp. 729–737.
[10] H.M. Diaz, C. Guedes Soares, A multi-criteria approach to evaluate floating offshore wind farms siting in the Canary Islands (Spain), Energies 14 (2021) 865.
[11] C.M. Goodess, A. Troccoli, C. Acton, J.A. Añel, P.E. Bett, D.J. Brayshaw, M. De Felice, S.R. Dorling, L. Dubus, L. Penny, B. Percy, T. Ranchin, C. Thomas, M. Trolliet, L. Wald, Advancing climate services for the European renewable energy sector through capacity building and user engagement, Clim. Serv. 16 (2019), 100139, 2019, 2405–8807.
[12] D.P. Dee, S.M. Uppala, A.J. Simmons, P. Berrisford, P. Poli, S. Kobayashi, U. Andrae, M.A. Balmaseda, G. Balsamo, P. Bauer, P. Bechtold, A.C.M. Beljaars, L. Van de Berg, J. Bidlot, N. Bormann, C. Delsol, R. Dragani, M. Fuentes, A.J. Geer, L. Haimberger, S.B. Healy, H. Hersbach, E.V. Hólm, L. Isaksen, P. Kållberg, M. Köhler, M. Matricardi, A.P. McNally, B.M. Monge-Sanz, J.-J. Morcrette, B.-K. Park, C. Peubey, P. Rosnay, C. Tavolato, F. Thépaut, J.-N. Vitart, The ERA-Interim reanalysis: configuration and performance of the data assimilation system, Q. J. R. Meteorol. Soc. 137 (2011) 553–597.
[13] Copernicus Climate Change Service ERA5 Monthly Averaged Data on Single Levels from 1979 to Present ECMWF, 2019.
[14] R. Gelaro, W. McCarty, M.J. Suárez, R. Todling, A. Molod, L. Takacs, C.A. Randles, A. Darmenov, M.G. Bosilovich, R. Reichle, K. Wargan, L. Coy, r R. Cullathe, C. Draper, S. Akella, V. Buchard, A. Conaty, A.M. da Silva, W. Gu, G.-K. Kim, R. Koster, R. Lucchesi, D. Merkova, J.E. Nielsen, G. Partyka, S. Pawson, W. Putman, M. Rienecker, S.D. Schubert, M. Sienkiewicz, B. Zhao, The modern-era retrospective analysis for research and applications, version 2 (MERRA-2), J. Clim. 30 (14) (2017) 5419–5454.
[15] I. González-Aparicio, F. Monforti, P. Volker, A. Zucker, F. Careri, T. Huld, J. Badger, Simulating European wind power generation applying statistical downscaling to reanalysis data, Appl. Energy 199 (2017) 155–168.
[16] K. Gruber, P. Regner, S. Wehrle, M. Zeyringer, J. Schmidt, Towards global validation of wind power simulations: a multi-country assessment of wind power simulation from MERRA-2 and ERA-5 reanalysis bias-corrected with the global wind atlas, Energy 238 (2022), 121520. Part A.
[17] S. Al-Yahyai, Y. Charabi, A. Gastli, Review of the use of numerical weather prediction (NWP) models for wind energy assessment, Renew. Sustain. Energy Rev. 14 (9) (2010) 3192–3198.
[18] N. Salvação, C. Guedes Soares, in: L. Castro-Santos, V. Diaz-Casas (Eds.), Resource Assessment Methods in the Offshore Wind Energy Sector, Floating Offshore Wind Farms, Springer International Publishing Switzerland, 2016, pp. 121–141.
[19] N. Salvação, M. Bernardino, C. Guedes Soares, Assessing mesoscale wind simulations in different environments, Comput. Geosci. 71 (2014) 28–36. October 2014.
[20] F.D. Jesus, M. Menéndez, R. Guanche, I. Losada, A wind chart to characterize potential offshore wind energy sites, Comput. Geosci. 71 (2014) 62–72.
[21] Y. Charabi, S. Al-Yahyai, A. Gastli, Evaluation of NWP performance for wind energy resource assessment in Oman, Renew. Sustain. Energy Rev. 15 (3) (2011) 1545–1555.
[22] I. Karagali, M. Badger, A.N. Hahmann, A. Peña, C.B. Hasaber, A.M. Sempreviva, Spatial and temporal variability of winds in the Northern European Seas, Renew. Energy 57 (2013) 200–210.
[23] N. Nawri, G.N. Petersen, H. Bjornsson, A.N. Hahmann, K. Jónasson, C.B. Hasager, N.-E. Clausen, The wind energy potential of Iceland, Renew. Energy 69 (2014) 290–299.
[24] N. Salvação, C. Guedes Soares, Wind resource assessment offshore the Atlantic Iberian coast with the WRF model, Energy 145 (2018) 276–287.
[25] S. Al-Yahyai, Y. Charabi, A. Al-Badi, A. Gastli, Nested ensemble NWP approach for wind energy assessment, Renew. Energy 37 (2012) 150–160.
[26] M.P. Mylonas, S. Barbouchi, H. Herrmann, P.T. Nastos, Sensitivity analysis of observational nudging methodology to reduce error in wind resource assessment (WRA) in the North Sea, Renew. Energy 120 (2018) 446–456.
[27] N.G.-A. Linaje, C. Mattar, D. Borvarán, Quantifying the wind energy potential differences using different WRF initial conditions on Mediterranean coast of Chile, Energy 188 (2019), 116027.
[28] J. Zhao, Y. Guo, X. Xiao, J. Wang, D. Chi, Z. Guo, Multi-step wind speed and power forecasts based on a WRF simulation and an optimized association method, Appl. Energy 197 (2017) 183–202.
[29] N. Naidu, G. Nagababu, S. Kachhwaha, V. Savsani, Evaluation of offshore wind power potential of India by combining satellite and moored buoy data, in: C. Guedes Soares (Ed.), Progress in Renewable Energies Offshore, Taylor & Francis Group, London, UK, 2016, pp. 153–158.
[30] S.V.A. Kumar, G. Nagababu, R. Kumar, Comparative study of offshore winds and wind energy production derived from multiple scatterometers and met buoys, Energy 185 (2019) 599–611.
[31] Q. Guo, R. Huang, L. Zhuang, K. Zhang, J. Huang, Assessment of China's offshore wind resources based on the integration of multiple satellite data and meteorological data, Rem. Sens. 11 (22) (2019) 2680.
[32] R. Chang, R. Zhu, M. Badger, C. Hasager, X. Xing, Y. Jiang, Offshore wind resources assessment from multiple satellite data and WRF modeling over south China sea, Rem. Sens. 7 (1) (2015) 467–487.
[33] C.B. Hasager, A.N. Hahmann, T. Ahsbahs, I. Karagali, T. Sile, M. Badger, J. Mann, Europe's Offshore Winds Assessed from SAR, ASCAT and WRF, Wind Energy Science, 2019, https://doi.org/10.5194/wes-2019-38.
[34] Q. Guo, X. Xu, K. Zhang, Z. Li, W. Huang, L. Mansaray, J. Huang, Assessing global ocean wind energy resources using multiple satellite data, Rem. Sens. 10 (2) (2018) 100.
[35] M.M. Nezhad, D. Groppi, P. Marzialetti, L. Fusilli, G. Laneve, F. Cumo, D.A. Garcia, Wind energy potential analysis using Sentinel-1 satellite: a review and a case study on Mediterranean islands, Renew. Sustain. Energy Rev. 109 (2019) 499–513.
[36] D. Carvalho, A. Rocha, M. Gómez-Gesteira, C.S. Santos, Offshore winds and wind energy production estimates derived from ASCAT, OSCAT, numerical weather prediction models and buoys – a comparative study for the Iberian Peninsula Atlantic coast, Renew. Energy 102 (2017) 433–444.
[37] D. Carvalho, A. Rocha, M. Gómez-Gesteira, I. Alvarez, C.S. Santos, Comparison between CCMP, QuikSCAT and buoy winds along the Iberian Peninsula coast, Rem. Sens. Environ. 137 (2013) 173–183.
[38] F. Santos, M. Gómez-Gesteira, M. deCastro, J.A. Añel, D. Carvalho, J.M. Dias, On the accuracy of CORDEX RCMs to project future winds over the Iberian Peninsula and surrounding ocean, Appl. Energy 228 (2018) 289–300, https://doi.org/10.1016/j.apenergy.2018.06.086.
[39] R.M. Campos, C. Guedes Soares, Spatial distribution of offshore wind statistics on the coast of Portugal using Regional Frequency Analysis, Renew. Energy 123 (2018) 806–816.
[40] J. Wang, S. Qin, S. Jin, J. Wu, Estimation methods review and analysis of offshore extreme wind speeds and wind energy resources, Renew. Sustain. Energy Rev. 42 (2015) 26–42.
[41] www.emodnet.eu.
[42] C.W. Fairall, E.F. Bradley, J.E. Hare, A.A. Grachev, J.B. Edson, Bulk parameterization of air–sea fluxes: updates and verification for the COARE algorithm, J. Clim. 16 (4) (2003) 571–591.
[43] W. Wang, D. Barker, J. Bray, C. Bruyere, M. Duda, J. Dudhia, User's Guide for Advanced Research WRF (ARW) Modeling System Version 3. Mesoscale and Microscale Meteorology Division, National Center for Atmospheric Research (MMM-NCAR), 2007.
[44] A. Bentamy, A. Mouche, A. Grouazel, A. Moujane, A.A. Mohamed, Using sentinel-1A SAR wind retrievals for enhancing scatterometer and radiometer regional wind analyses, Int. J. Rem. Sens. 40 (3) (2018) 1120–1147.
[45] F. Desbiolles, A. Bentamy, B. Blanke, C. Roy, A.M. Mestas-Nuñez, S.A. Grodsky, S. Herbette, G. Cambon, C. Maes, Two decades [1992–2012] of surface wind analyses based on satellite scatterometer observations, J. Mar. Syst. 168 (2017) 38–56.
[46] F.J. Wentz, SSM/I Version-7 Calibration Report, Remote Sensing Systems, Santa Rosa, CA, 2013, p. 46, report number 011012.
[47] A. Bentamy, D. Croize-Fillon, C. Perigaud, Characterization of ASCAT measurements based on buoy and QuikSCAT wind vector observations, Ocean Sci. 4 (4) (2008) 265–274.
[48] G. Gómez, W.D. Cabos, G. Liguori, D. Sein, S. Lozano-Galeana, L. Fita, J. Fernández, M.E. Magariño, P. Jimenez-Guerrero, J.P. Montávez, M. Dominguez, R. Romera, M. Gaertner, Characterization of the wind speed variability and future change in the Iberian Peninsula and the Balearic Islands, Wind Energy 19 (7) (2015) 1223–1237.

[49] P. Patlakas, G. Galanis, N. Barranger, G. Kallos, Extreme wind events in a complex maritime environment: ways of quantification, J. Wind Eng. Ind. Aerod. 149 (2016) 89–101.
[50] A.N. Hahmann, T. Sīle, B. Witha, N.N. Davis, M. Dörenkämper, Y. Ezber, E. García-Bustamante, J.F. González-Rouco, J. Navarro, B.T. Olsen, S. Söderberg, The making of the new European wind atlas – Part 1: model sensitivity, Geosci. Model Dev. (GMD) 13 (10) (2020) 5053–5078.
[51] H. Bailey, K. Brookes, P. Thompson, Assessing environmental impacts of offshore wind farms: lessons learned and recommendations for the future, Aquat. Biosyst. 10 (2014) 8, https://doi.org/10.1186/2046-9063-10-8.
[52] A. Al-Hinai, Y. Charabi, S.H. Aghay Kaboli, Offshore wind energy resource assessment across the territory of Oman: a spatial-temporal data analysis, Sustainability 13 (2021) 2862.
[53] E. Dupont, R. Koppelaar, H. Jeanmart, Global available wind energy with physical and energy return on investment constraints, Appl. Energy 209 (2017), https://doi.org/10.1016/j.apenergy.2017.09.085.
[54] S. Jerez, R.M. Trigo, S.M. Vicente-Serrano, D. Pozo-Vázquez, R. Lorente-Plazas, J. Lorenzo-Lacruz, F. Santos-Alamillos, J.P. Montávez, The impact of the north Atlantic Oscillation on renewable energy resources in Southwestern Europe, J. Appl. Meteorol. Climatol. 52 (10) (2013) 2204–2225.
[55] P.M.M. Soares, R.M. Cardoso, A. Semedo, M.J. Chinita, R. Ranjha, Climatology of the Iberia coastal low-level wind jet: weather research forecasting model high-resolution results, Tellus Dyn. Meteorol. Oceanogr. 66 (1) (2014), 22377.
[56] K.-Y. Oh, J.-Y. Kim, J.-S. Lee, K.-W. Ryu, Wind resource assessment around Korean Peninsula for feasibility study on 100 MW class offshore wind farm, Renew. Energy 42 (2012) 217–226.
[57] N. Salvação, C. Guedes Soares, A. Bentamy, Estimating the offshore wind energy along the Portuguese coast using WRF and satellite data, in: C. Guedes Soares (Ed.), Advances in Renewable Energies Offshore, Taylor & Francis Group, London, UK, 2019, pp. 703–710.
[58] S. Salvador, L. Gimeno, F. Javier Sanz Larruga, The influence of maritime spatial planning on the development of marine renewable energies in Portugal and Spain: legal challenges and opportunities, Energy Pol. 128 (2019) 316–328. ISSN 0301-4215.